Journal of
Manufacturing and Materials Processing

MDPI

Article

Investigation of Digital Light Processing-Based 3D Printing for Optimized Tooling in Automotive and Electronics Sheet Metal Forming

Szabolcs Szalai [1], Brigitta Fruzsina Szívós [1], Vivien Nemes [1], György Szabó [1], Dmytro Kurhan [2], Mykola Sysyn [3] and Szabolcs Fischer [1,*]

[1] Central Campus Győr, Széchenyi István University, H-9026 Győr, Hungary; szalaisz@sze.hu (S.S.); szivos.brigitta.fruzsina@sze.hu (B.F.S.); nemes.vivien@sze.hu (V.N.); gyorgyszabo86@gmail.com (G.S.)
[2] Department of Transport Infrastructure, Ukrainian State University of Science and Technologies, UA-49005 Dnipro, Ukraine; d.m.kurhan@ust.edu.ua
[3] Department of Planning and Design of Railway Infrastructure, Technical University Dresden, D-01069 Dresden, Germany; mykola.sysyn@tu-dresden.de
* Correspondence: fischersz@sze.hu; Tel.: +36-(96)-503-400

Abstract: This study addresses the emerging need for efficient and cost-effective solutions in low-volume production by exploring the mechanical performance and industrial feasibility of cutting tools that are fabricated using stereolithography apparatus (SLA) technology. SLA's high-resolution capabilities make it suitable for creating precise cutting dies, which were tested on aluminum sheets (Al99.5, 0.3 mm, and AlMg3, 1.0 mm) under a 60-ton hydraulic press. Measurements using digital image correlation (DIC) revealed minimal wear and deformation, with tolerances consistently within IT 0.1 mm. The results demonstrated that SLA-printed tools perform comparably to conventional metal tools in cutting and bending operations, achieving similar surface quality and edge precision while significantly reducing the production time and cost. Despite some limitations in wear resistance, the findings highlight SLA technology's potential for rapid prototyping and short-run manufacturing in the automotive and electronics sectors. This research fills a critical gap in understanding SLA-based tooling applications, offering insights into process optimization to enhance tool durability and broaden material compatibility. These advancements position SLA technology as a transformative tool-making technology for flexible manufacturing.

Keywords: 3D printing; SLA; rapid prototype; 3D scanning; optimization; part-off die; cut-off die; DIC; GOM ATOS; sheet metal

Academic Editor: Shuo Yin

Received: 7 November 2024
Revised: 10 January 2025
Accepted: 14 January 2025
Published: 15 January 2025

Citation: Szalai, S.; Szívós, B.F.; Nemes, V.; Szabó, G.; Kurhan, D.; Sysyn, M.; Fischer, S. Investigation of Digital Light Processing-Based 3D Printing for Optimized Tooling in Automotive and Electronics Sheet Metal Forming. *J. Manuf. Mater. Process.* **2025**, *9*, 25. https://doi.org/10.3390/jmmp9010025

1. Introduction

Sheet metal forming is extensively utilized across industries, including automotive, railway vehicle manufacturing, aerospace, shipbuilding, watchmaking, and more [1,2]. Typically employed for large-scale production, this process necessitates costly tooling [1]. However, the financial and technical challenges can be mitigated by simplifying the tool manufacturing process [1] or employing specialized optimization techniques [3,4].

Flat sheets can be transformed into complex three-dimensional parts using methods like bending and deep drawing [5]. More advanced processes include welding [6], bolting, adhesive bonding [7], and clip applications [8,9]. Sheet metal forming offers advantages such as favorable mechanical properties of the final part, minimal material waste, and a

high production capacity. However, the primary disadvantages are the significant costs and time that are required to establish a new production line.

During the development of tools, multiple iterations may be necessary to achieve the final design. Each revision incurs additional machining and processing costs, escalating both the monetary and temporal investments. Consequently, sheet metal forming is predominantly reserved for mass production to maintain cost-effectiveness [5].

The global smart manufacturing industry is undergoing substantial shifts due to heightened competition, requiring significant adaptations [10]. Advancing the manufacturing sector involves exploring innovative processes, materials, and production technologies. Traditional manufacturing workflows involve numerous interdependent tools and processes, resulting in complex operations, extended production times, and high costs—primarily suited to mass or standardized production [10].

Industries are increasingly prioritizing customized manufacturing, spurring demand for small-batch production, where adaptable bending tools are essential [11]. Recently, advancements in additive manufacturing (AM) technologies and materials have bolstered the interest in flexible, rapid tooling. The imperative to minimize the production time and costs underscores the demand for efficient, responsive tooling for prototype and short-term production needs [11].

AM represents the most advanced manufacturing approach, revolutionizing numerous industries [12]. Key benefits of AM include a substantial material waste reduction, shorter production timelines, the elimination of complex tooling, lower energy consumption, and the ability to produce intricate designs that are unachievable with traditional methods [12].

This evolution has introduced rapid tooling technologies, such as 3D printing, which employs advanced polymers and composite materials to fabricate tools for sheet metal forming [11]. Emerging market demands for mass customization and technological innovations have intensified the interest in additive technologies like 3D printing [13,14]. AM of tools for casting, injection molding, metal forming, and similar applications has become an industrial standard [13,14].

Unlike traditional methods, 3D printing can produce diverse part geometries without auxiliary machines, molds, or fixtures [10]. For instance, railway ballast aggregates have been successfully 3D-printed [15,16]. This makes 3D printing an excellent solution for small-batch production and personalized customization. Its automated, high-precision capabilities enable the rapid creation of complex shapes, such as freeform surfaces. The cutting process generates no waste, reducing resource usage and material costs. Moreover, 3D printing allows for the direct production of intricate parts from digital models, significantly shortening product development cycles. Enhanced material utilization rates further demonstrate 3D printing's unmatched advantages in automated precision manufacturing [10].

Three-dimensional printing constructs three-dimensional solid objects from digital files [17]. This process, achieved through successive material layering, begins with a 3D model, typically designed using computer-aided design (CAD). The model is sliced into cross-sectional layers, generating a file for the 3D printer, which builds the object layer by layer [17].

Several 3D printing systems exist [18,19]. Among the most prominent is the stereolithography apparatus (SLA), which employs a high-powered laser to cure liquid resin into the desired 3D shape. The SLA uses two-dimensional cross-sections from CAD data, curing them layer by layer through UV laser photopolymerization [18,19].

Digital light processing (DLP) differs from SLA technology in that it cures entire resin layers simultaneously rather than tracing them with a laser, making DLP faster than SLA technology [20–22]. Both technologies deliver exceptional resolution, producing highly accurate parts [20–22].

SLA technology is increasingly popular due to its dimensional accuracy and superior part quality compared to fused deposition modeling (FDM®) [23]. A broad range of SLA-printable resins further enhances its competitiveness in mechanical engineering [23].

SLA technology surpasses other low-cost 3D printing technologies like FDM® by offering a higher dimensional accuracy, smoother finishes, faster speeds, watertight parts, isotropic material behavior, and user-friendly operation [23]. Unlike top-down systems, SLA technology's bottom-up approach minimizes oxygen interference during polymerization, ensuring consistent curing [23].

SLA-printed parts generally exhibit minimal warping, primarily during post-processing [23]. Their surface quality depends significantly on the layer height, particularly for inclined surfaces. Compared to FDM®, SLA technology produces parts with nearly invisible layer junctions, resulting in smoother finishes and better mechanical properties. FDM® parts, by contrast, often feature unavoidable micro-gaps that increase cracking risks due to surface roughness. SLA parts are less susceptible to such defects, enhancing their durability [23].

Both FDM® and SLA technology enable the precise production of intricate structures, although SLA technology is preferred for complex, highly accurate shapes [24]. Mechanical evaluations, including tensile and bending tests, reveal that SLA-printed parts outperform FDM® parts in terms of strength and durability [24]. SLA components consistently exhibit superior mechanical performance, reinforcing their advantages in demanding applications [24].

Critical factors influencing printed parts' properties include their layer thickness, hatch spacing, and laser beam width [25]. Comparative studies of SLA technology, DLP, continuous digital light processing (cDLP), and pulse projection polymerization (PPP) show that SLA technology provides the highest accuracy, with 94.9% of measured points being within predefined tolerances [18].

While FDM® demonstrates greater systematic deviations (158.1 µm) than SLA technology (109.9 µm), SLA molds typically exhibit less distortion [26]. Benchmark studies evaluating different 3D printers indicate that SLA technology achieves lower geometric deviations, although environmental conditions like temperature and humidity affect the results of both processes [19].

Mechanical anisotropy, which is inherent in 3D-printed parts, leads to varying properties based on orientation [12]. SLA technology minimizes anisotropy by forming bonds axially and transversely during printing, creating isotropic properties. However, slight mechanical differences (up to 10%) may arise due to printer movements [27].

SLA printing is constrained by the build volume, necessitating efficient space utilization for maximum production. Anisotropic effects can influence the build times and manufacturing efficiency. Understanding this behavior is vital for strategic production planning [28].

Research suggests that SLA parts are isotropic, offering consistent properties across orientations, giving SLA technology a significant advantage over anisotropic technologies like FDM® [12]. The tensile strength correlates with print orientation, decreasing with increased angles, while Young's modulus remains relatively consistent, reinforcing SLA technology's isotropy [25].

Rubber pad forming, involving elastic materials like polyurethane paired with steel counterparts, has advanced in sheet metal forming. It enhances the workpiece formability and enables various operations, including blanking and bending [29,30]. While economical for small-scale production, rubber tooling has limitations, such as deformation during use and high forming force requirements [29].

Rubber tooling is well suited for thin sheet blanking, cutting aluminum sheets up to 1.5 mm thick. However, it produces a significant amount of waste and has limited dimensional accuracy [31]. Material separation involves bending and tearing, and the

optimal cutting die heights to minimize burr formation can be calculated using established equations [30]. The optimal height of the cutting die for minimizing burr formation can be calculated using Equation (1).

$$H = 3\left(1 + \frac{A_{11.3}}{100}\right)\sqrt{s}\ [\text{mm}] \quad (1)$$

where s is the thickness of the plate (sheet) in mm, and $A_{11.3}$ is the percentage strain at breakage related to an $L_o = 10 \cdot d_0$ measuring basis (base) length (d_0 represents the original diameter (or thickness) of the sample or specimen used in the tensile test before any deformation occurs) [31,32].

One of its advantages lies in the processing of thin sheets [32]. For cutting or punching of thin sheets (with a thickness below 0.5 mm), the cutting–punching tool must be manufactured with high precision due to the small allowable clearance. Uneven positioning or a huge clearance can result in burrs on the workpiece, which are extremely difficult to remove from delicate components [32].

The shape accuracy of parts that were cut from a 0.5 mm thick Al99.5 sheet material and had holes punched through them was investigated [32]. The results showed excellent shape accuracy for the cut parts, with the corner rounding of the square shapes being less than 0.1 mm. For square-punched parts, the corner rounding radius was found to be 1.0 mm [32].

This section has presented various 3D printing technologies and their application areas. This summary highlights that although these technologies are widely used, their application as base materials for cutting tools in sheet metal cutting has not yet been explored. The novelty of the current research lies in this aspect, as its primary focus is the study of 3D-printed cutting tools.

In this paper, the following sections will introduce the materials and methods used (Section 2), present the results of the investigations (Section 3), and discuss the results (Section 3). Finally, a brief summary will outline the conclusions derived from the findings and future plans (Section 4).

2. Materials and Methods

2.1. Materials

The experiments were conducted using two types of sheet materials: Al99.5 with a thickness of 0.3 mm and AlMg3 with a thickness of 1.0 mm.

Al99.5 is a high-purity aluminum alloy containing 99.5% pure aluminum. This material is highly suitable for applications requiring excellent corrosion resistance in neutral environments without chlorides, easy machinability, and superior thermal conductivity. Due to its low density (~2.70 g/cm^3), Al99.5 is exceptionally lightweight, making it an ideal choice in automotive, aerospace, and construction industries, where weight reduction is a critical consideration. While its strength and hardness are not as high as those of alloyed aluminum grades, it offers excellent formability, allowing it to be easily shaped and rolled. This property is particularly beneficial for sheet metal forming processes.

AlMg3 is an aluminum alloy with a medium magnesium content, containing approximately 3% magnesium. This alloy exhibits various desirable properties, making it suitable for diverse applications. It provides good corrosion resistance, especially in marine environments, where the natural oxide layer of aluminum combined with the magnesium addition enhances the resistance to saltwater and humid conditions. Mechanically, AlMg3 is stronger than pure aluminum while maintaining a low density (~2.66 g/cm^3), resulting in a lightweight yet relatively strong material. Its good formability makes it suitable for various forming processes, such as rolling and pressing. Additionally, AlMg3 demonstrates

excellent toughness, withstanding mechanical impacts and maintaining good deformation capability, even at low temperatures.

The 3D printing experiments utilized an Anycubic Photon Mono printer, employing DLP technology (manufacturer: Shenzhen Anycubic Technology Co., Ltd., Hong Kong, China). The Phrozen TR250LV resin, specially developed for industrial and engineering purposes, was selected for the printing tasks.

This resin is highly suited for producing functional prototypes and durable components. One of its key features is its low shrinkage, which ensures more stable and accurate printing results with minimal deformation. The Phrozen TR250LV resin offers high strength and stiffness, making it capable of withstanding mechanical loads and enabling the production of robust parts. It is particularly suitable for high-precision projects, including engineering components, industrial molds, and fixtures.

Additionally, the resin is compatible with multiple SLA and DLP printers, particularly in low-UV-light printing environments, enhancing its versatility. The main parameters of the resin are detailed in Table 1.

Table 1. The relevant characteristics of the applied resin according to the relevant standards [33–38].

Resin	Phrozen TR250LV	Standards
Weight [g/bottle]	1000.00	-
Density [g/cm^3]	1.10	D792 [33]
Viscosity [Pa × s]	230–300 × 10^{-3}	ISO 1628 [34]
Surface Hardness in Shore D	79.00	ISO 164 [35]
Tensile Stress at Break [MPa]	25.00	ISO 527 [36]
Tensile Modulus [MPa]	900.00	ISO 527 [36]
Elongation at Break [%]	20.00	ISO 527 [36]
Notched Izod Impact [J/m]	6.31	ISO 180 [37]
Heat Deflection Temperature at 0.45 MPa [°C]	80.00	D790 [38]

2.2. Instruments and Machines

Since the cutting die was produced using 3D printing, the following section provides an overview of the DLP-based 3D printer that was utilized.

The Anycubic Photon Mono is a popular DLP (digital light processing) 3D printer, known for its precision and ability to produce detailed prints. It features a 6-inch monochrome LCD screen, allowing for faster UV light transmission than conventional color LCDs. This significantly increases printing speeds—it is up to two to three times faster than earlier models—while extending the LCD's lifespan.

The Photon Mono printer employs DLP printing technology, which cures liquid resin with UV light. The process involves initial curing during the printing phase, followed by final curing in a UV chamber (see Figure 1). This results in smoother and more detailed prints compared to traditional FDM® printers. These characteristics make it an excellent choice for applications such as modeling, prototyping, and other tasks requiring fine details.

The main parameters of the printer are listed in Table 2.

For the measurement and comparison of the printed tools, a 3D laser scanner was employed [39]. Specifically, the GOM Atos TripleScan v2.0 system (manufacturer: Carl Zeiss IQS Deutschland GmbH, Braunschweig, Germany) was used in this research (see Figure 2).

The GOM Atos TripleScan system is an advanced optical 3D measurement tool, designed for precise surface digitization and measurement. It offers exceptional accuracy when analyzing complex geometries, fine details, and reflective surfaces. The TripleScan technology employs three different projection paths to scan the surface, minimizing the formation of shadows and blind spots. This ensures comprehensive and detailed data capture from multiple perspectives [40,41]. The applied GOM Atos TripleScan scanner, i.e., the

instrument, is regularly maintained and calibrated. Both the calibration of the instrument and the verification of the calibration plate are carried out at most annually. Before each measurement, a specific, accurate calibration procedure, as prescribed by the manufacturer, is carried out using the calibration plate, taking the temperature of the measurement and other local conditions into account. The manufacturer guarantees a measurement accuracy of 0.001 mm for these measurements.

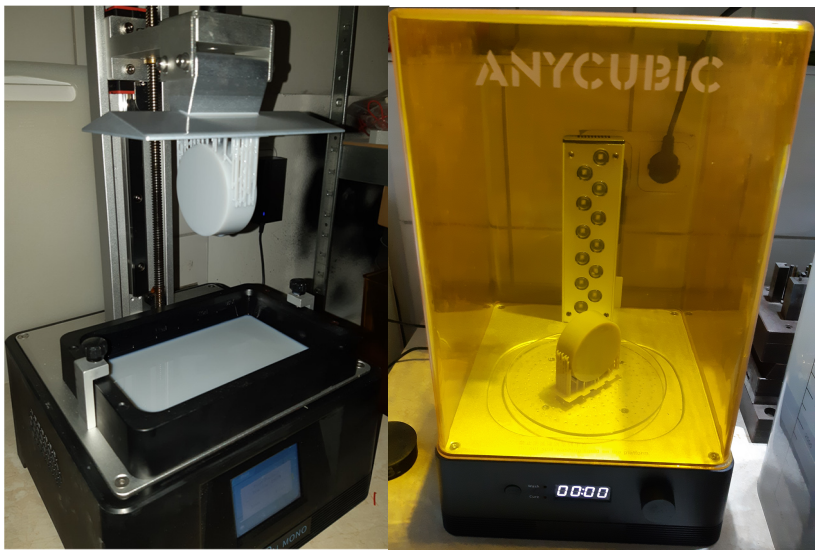

Figure 1. The Anycubic Photon Mono 3D printer and UV chamber used.

Table 2. Main parameters of Anycubic Photon Mono.

Printer	Anycubic Photon Mono
Technology	Digital light processing (DLP)
Build volume *XYZ*: [mm × mm × mm]	130.000 × 80.000 × 165.000
Display type [pixels × pixels]	2K (2560 × 1620) LCD
XY resolution [mm]	0.051
Z-axis resolution [mm]	0.010
Laser resolution [mm]	0.010. . .0.150
Printing speed [mm/h]	max. 50.000

Figure 2. The applied GOM Atos scanner.

The ATOS system is highly suitable for various industries, including automotive, aerospace, and plastic and tool manufacturing. It enables comprehensive 3D digitization of parts with complex geometries, facilitating quality control, reverse engineering, and optimization of development processes. The sensor provides high-resolution measurement results, delivering precise data on the shape and dimensions of products, which can be compared to reference models for thorough analysis.

An added advantage of the GOM ATOS TripleScan system is its ability to measure reflective materials, a unique feature compared to conventional 3D measurement systems. The measurement process is both fast and accurate, with automated data processing that expedites the evaluation of results. This significantly supports the reduction in product development cycles and ensures compliance with stringent manufacturing quality requirements [40,42].

Following the measurement of the tools, a Hidroma 60-ton hydraulic press (manufacturer: HYDROMA SK, Považská Bystrica, Czechoslovakia) was used for the experiments.

The Hidroma 60-ton (~600 kN) hydraulic press is a robust industrial machine, designed for various forming, pressing, and material processing tasks. It is particularly suited for shaping and refining metal components and performing other mechanical operations requiring high pressure. The 600 kN pressing force is sufficient for working with larger and thicker materials. The setup for the cutting process is shown in Figure 3 [40].

Figure 3. Cutting setup on the Hidroma Press.

The Hidroma press is exact and user-friendly and features a robust steel structure that ensures the machine's durability and reliability in industrial environments. Its simple controls allow users to quickly set the desired pressing force and accurately manage the processes. The device is also equipped with safety features to protect the operator and minimize the risk of accidents.

This hydraulic press type is advantageous in automotive repair shops, metalworking, and industrial production, where significant force is required for material forming [40].

2.3. Process

In the design of rubber pad tools, the equation developed by Komarov [30,32] is commonly used in both industry and the literature to achieve minimal burr formation. This equation determines the minimum cutting die height, which ensures optimal burr formation. The equation is presented in Equation (2).

$$H = 3(1 + 0.01 \times A_{11.3})\sqrt{s} \quad (2)$$

where H is the cutting die height. According to this equation, the required cutting die heights for the 0.3 mm thick Al99.5 sheet material and the 1.0 mm thick AlMg3 sheet material are shown in Table 3.

Table 3. Cutting die heights corresponding to sheet thicknesses.

	H (mm)	
s	**Al99.5 ($A_{11.3}$ = 50%)**	**AlMg3 ($A_{11.3}$ = 17%)**
0.3 mm	2.46	1.92
1.0 mm	4.50	3.51

This research primarily focuses on testing materials and technology while evaluating the low resolution that is achievable with DLP technology. Due to this limitation, the calculated minimum cutting die height values are very small, resulting in insufficient height. This increases the risk of cutting die breakage; therefore, the thickness of the cutting dies was uniformly set to 20 mm. To enable the testing of minimum height values, an adapter ring was designed with a test height of 10 mm, resulting in a material removal zone height of 10 mm. With these settings, burr formation is expected to increase, but the cutting process will remain analyzable. Another parameter of the cutting die is the side taper angle, which was not calculated but taken from the literature and was uniformly set to 4°. The cross-sections of the designed tools are shown in Figure 4.

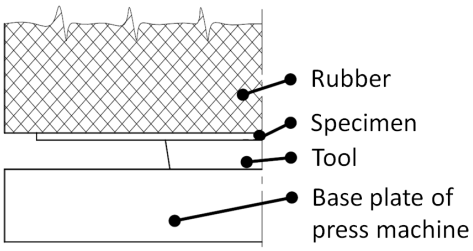

Figure 4. Cross-section of the designed tools.

Unlike FDM® technology, DLP printers offer significantly fewer customization options in the 3D printer's slicer software (Anycubic Photon Workshop 3.5.0). Typically, users can adjust parameters such as the layer height, number of bottom layers, exposure times for different layer types, and movement speeds. However, manufacturers provide predefined settings that are specific to the printer and resin types.

During the printing of the tool, the settings recommended by the resin manufacturer were applied, with only minor deviations in a few areas. The values recommended by the manufacturer are listed in Table 4.

Table 4. Recommended printing characteristics (parameters) of the manufacturer of the applied resin.

Recommended Settings—Phrozen	Settings	Value
Burn-in Layers	Number of layers [pcs]	6
	Exposure time [s]	30.00
Normal Layers	Layer thickness [µm]	50.00
	Light-off delay [s]	1.50
	Exposure time [s]	2.30
	Lift distance [mm]	5.00
Speed	Lift speed [mm/s]	1.00
	Retraction speed [mm/s]	1.50
Print Time Override	Time per burn-in layer [s]	0.00
	Time per layer [s]	0.00

The layer height was set to 0.05 mm. Research supports that the smaller a layer thickness a DLP printer uses, the greater the achievable geometric accuracy is [42]. The

number of base layers remained at the default value of six. The importance of the initial layers lies in ensuring the model's adhesion to the build plate, which must be strong enough to prevent detachment during printing. Optimizing this involves adjusting the exposure time, during which the curing of the bottom layers occurs. Since this parameter is critical and the manufacturer provides no explicit value, test prints were conducted to determine the optimal setting, and the exposure time was adjusted to 35 s to eliminate the risk of the solid tool detaching from the build plate.

One distinctive feature of the Anycubic Photon Mono is its monochrome display, allowing for relatively short exposure times for layers beyond the initial ones. With the printer's higher brightness and resolution (Full HD 4K), shorter exposure times than those recommended are sufficient; thus, the exposure time was set to 2.5 s.

Regarding the print orientation, DLP technology is much less sensitive to mechanical properties, as the material loses the anisotropy that is inherent to layered construction during curing, acquiring isotropic properties. The model was positioned perpendicularly to the build plate, with an infill pattern set to "Cubic" and a 100% infill density. Since 100% infill affects the model's weight, adequate support structures were added.

Tools that were printed using DLP technology required several post-processing steps. First, after removing the build plate, the models were placed in a washer filled with isopropanol for 20 min to dissolve and wash away any uncured resin from their surfaces. Following washing, the tools were placed in a closed UV chamber for 25 min to ensure complete resin curing. Once cured, the support structures could be easily removed with minimal force, and any remaining residues were smoothed out with fine sandpaper. Figure 5 shows the model before support removal (left) and the finalized, cleaned model (right).

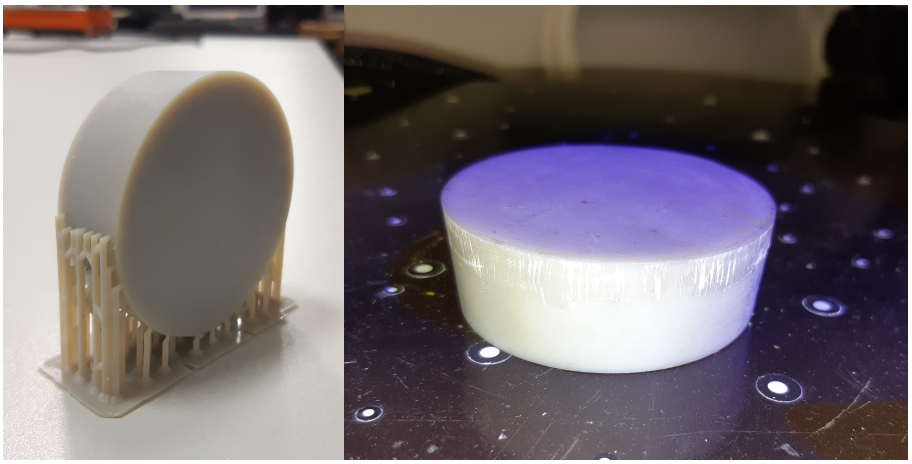

Figure 5. The model with support (**left**) and the tool in state 0 (**right**).

During the testing process, the initial step involved measuring each cutting die's zero state (pre-cutting condition) using the GOM Atos system, capturing complete 3D models. Subsequently, three samples were cut from each sheet material. Another Atos measurement followed the first round of cutting. After this, an additional three samples were cut, again followed by measurement.

The reference point for the color map analysis was the zero state measurement, against which the post-cutting states were compared. The base alignment for all measurements used the "best fit" orientation. The primary focus during the evaluation was on edge wear and changes in the cutting die geometry.

After the normal measurements, stepped or loading tests were conducted. Here, the cutting dies were used to cut three 0.3 mm thick sheets and then three 1.0 mm thick sheets, with the cutting process being controlled by operators using the Hidroma press. This

allowed for the investigation of the effects of increasing the load and wear. At the end of the cutting process, another GOM Atos measurement was performed under the same settings as in the normal measurements.

Measurement matrix (see Table 5):

R1-1; R1-2; R1-3: Normal, for 0.3 mm thick sheets.

R2-1; R2-2; R2-3: Normal, for 1.0 mm thick sheets.

R3-1; R3-2; R3-3: Loading, for 0.3 mm and 1.0 mm thick sheets.

Table 5. Measurement matrices of tools.

Specimens	Sheet (Plate) Thickness [mm]	State	Measurement	Number of Pieces
R1	-	0 (ref.)	yes	3
	0.3	3 (after 3 cuttings)	yes	3
	0.3	6 (after 6 cuttings)	yes	3
R2	-	0 (ref.)	yes	3
	1.0	3 (after 3 cuttings)	yes	3
	1.0	6 (after 6 cuttings)	yes	3
R3	-	0 (ref.)	yes	3
	0.3	3 (after 3 cuttings)	yes	3
	1.0	6 (after 6 cuttings)	yes	3

3. Results and Discussion

During the testing of the DLP cutting dies, each die was tested three times for the successful cutting of 0.3 mm thick Al99.5 aluminum sheets. The post-cutting states were measured using the GOM ATOS system and compared to the initial zero state to analyze the burr formation and edge wear. The cutting dies were also tested in three sets for the 1.0 mm thick AlMg3 sheet material. The dies successfully completed the cutting process for this material as well. After cutting, the geometries of the measured tools were compared with their zero states to determine the edge wear associated with the 1 mm thick sheet material.

Since the cuts for both the 0.3 mm Al99.5 and the 1.0 mm AlMg3 sheets were successful, further testing was conducted to assess the durability of the tool design after cutting both sheet thicknesses. Tools that were previously used for cutting the 0.3 mm sheets were tested on the 1.0 mm thick sheets to evaluate whether the worn tools could handle the thicker material. The experiments were successful, with each tool completing three successful cuts on three sheets.

Thus, tools that had cut a total of six sheets were measured using the GOM ATOS system, and the cumulative tool wear was evaluated.

After the DIC (digital image correlation) measurement, the same tools underwent another test series on 1.0 mm thick AlMg3 sheets. In all three instances, the cutting operations were successfully performed again (Figure 6).

The test series concluded that most tools performed exceptionally well. In many cases, the cut workpieces displayed high-quality contours. Burr formation was either nonexistent or minimal for specific tools, as shown in Figure 7.

The degree of burr formation can be defined as follows: minimal—barely perceptible by touch, ranging from 0.01 to 0.05 mm; moderate—clearly perceptible by touch, yet post-processing may not be necessary, ranging from 0.05 to 0.1 mm; significant burr—visibly and palpably sharp, posing a risk of injury, exceeding 0.1 mm. In some cuts, minimal or moderate burr formation was observed. This is likely partly due to human factors during the pressing process, as the relative positions of the tool, sheet, rubber pads, and pressing element vary slightly with each press. Figure 8 illustrates some examples of successful cuts.

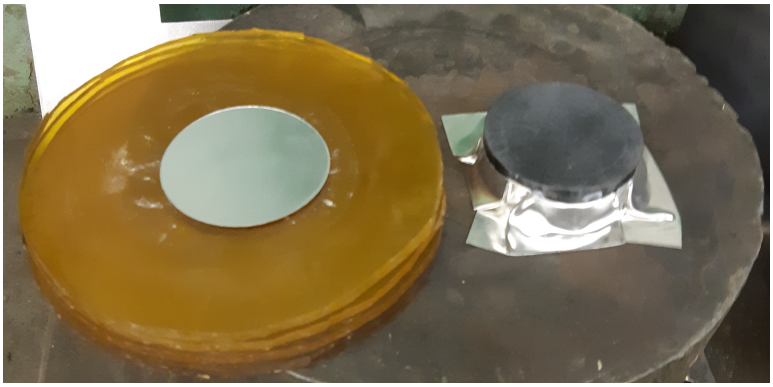

Figure 6. An image of the successful cutting.

Figure 7. Burr-free cutting experiment.

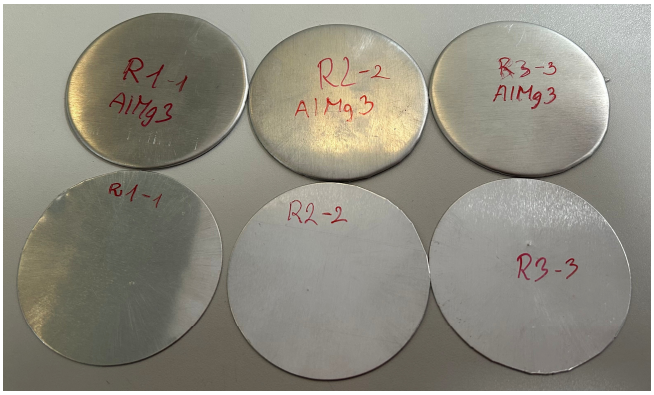

Figure 8. Examples of the successful cutting procedure.

Two evaluations were conducted for the DLP-manufactured cutting dies. The first evaluation followed three cuts of 0.3 mm thick Al99.5 H24 sheets. These cuts were of good quality, with minimal or no burr formation. The evaluation showed an average edge wear of +0.02 mm.

The second evaluation of the resin-based tool followed three cuts of 1.0 mm thick AlMg3 sheets. The cuts for this thickness were also of acceptable quality, with an average edge wear of –0.02 mm (Tables 6 and 7). Data regarding the edge wear of the resin (R1) cutting tools are summarized in Table 8.

Figure 9 shows the measurement points. Measurements were taken at four points along the cutting edges, with each point being measured three times per series. The

tables present the averages of these measurements, meaning that each value represents the average of three measurements per point in three test series (e.g., R1-1, R1-2, R1-3).

The following image series (Figures 10 and 11) displays the R3 series samples following cuts of 0.3 mm and 1.0 mm sheets. Although the tables only report results from the four measured points on the cutting edge, the DIC images reveal additional phenomena. These findings are also reflected in Tables 6–8.

Table 6. Measurement results for 0.3 mm thick Al99.5 sheets (M1. . .M4 are defined in Figure 9).

ID	Status	Thickness [mm]	M1	M2	M3	M4
R1	0	-	0.01	0	0	−0.01
R1	3	0.3	0	0	−0.04	−0.02
R1	6	0.3	0	0	−0.06	−0.02

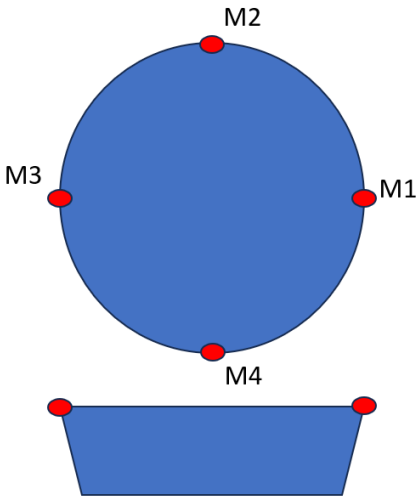

Figure 9. Measuring points (M1. . .M4).

Table 7. Measurement results for 1.0 mm thick Al99.5 sheets (M1. . .M4 are defined in Figure 9).

ID	Status	Thickness [mm]	M1	M2	M3	M4
R2	0	-	0.01	0.01	0	−0.01
R2	3	1	−0.01	0	−0.02	−0.03
R2	6	1	−0.02	0	−0.03	−0.05

Table 8. Measurement results from the loading tests (M1. . .M4 are defined in Figure 9).

ID	Status	Thickness [mm]	M1	M2	M3	M4
R3	0	-	0.01	0.02	−0.01	−0.01
R3	3	0.3	0	0.01	0	−0.02
R3	6	1	−0.03	−0.01	−0.04	−0.06

The presented results clearly demonstrate that the edge wear remained below 0.05–0.08 mm across all cutting edges, even during the loading tests (not only at the measurement points but also in the ColorPlot evaluations). For similar tools made from metal, the expected tolerance of workpieces falls around IT10-IT11 (ISO 286-1) [43], which, depending on size, ranges between 0.05 mm and 0.1 mm. It can be concluded that tools produced with this technology can meet the required manufacturing tolerances for small-batch production. None of the test pieces exhibited worse than moderate burr formation, aligning well with the technology's capabilities.

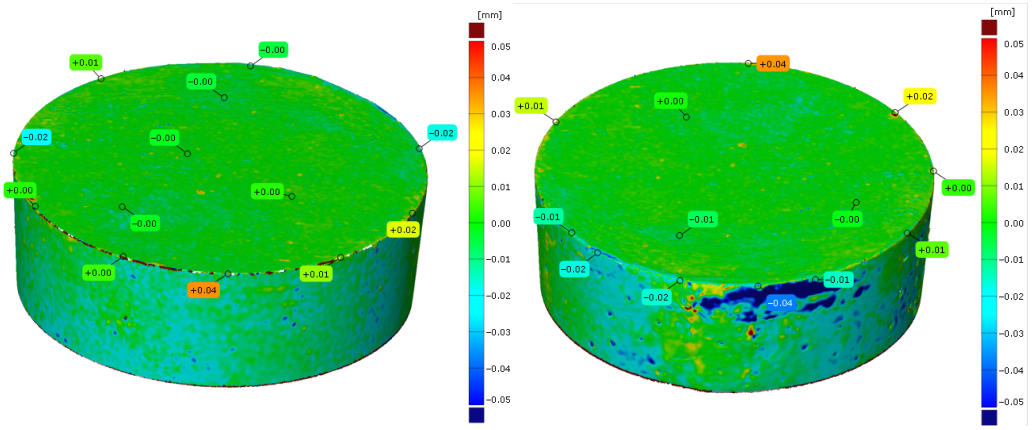

Figure 10. Results of the DIC analyses after cutting of thin sheets (s = 0.3 mm).

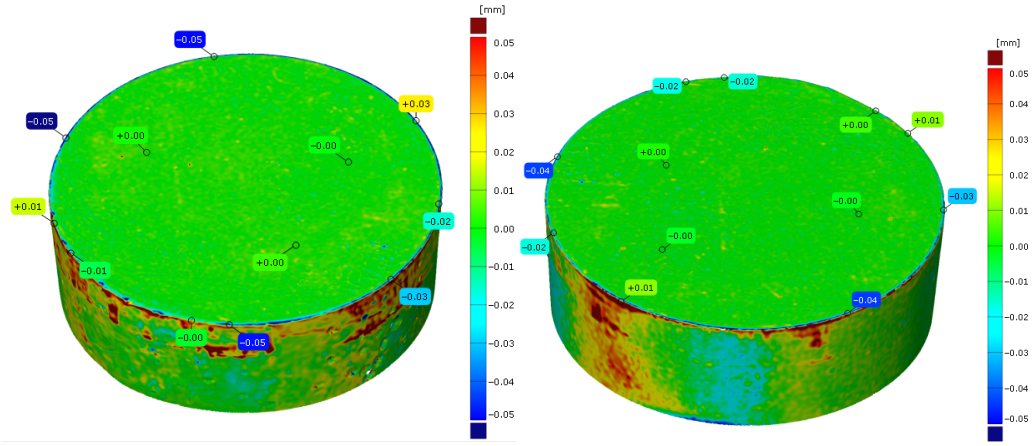

Figure 11. Results of the DIC analyses after cutting of thick sheets (s = 1.0 mm).

The question may be raised whether the measured values between 0.00 and 0.06 mm given in Tables 6–8 and Figures 10 and 11 are the actual, precise, accurate wear deformations or the measurement noise of the GOM Atos TripleScan system (see Section 2.2, specifically the paragraph above Figure 2). Taking these into account, the influence of measurement noise in the given range of values (0.00–0.06 mm) can be completely excluded, because the accuracy of the instrument is 0.001 mm.

4. Conclusions

This research confirms the suitability of DLP-based 3D printing technology for producing cutting tools that can be used in low-volume manufacturing, especially in the automotive and electronics industries. The study demonstrated that DLP-printed tools achieve mechanical performances that are comparable to traditional metal tools, meeting international tolerance standards (IT10–IT11) with minimal burr formation [43]. These results validate the potential of DLP technology to address critical challenges in small-batch production, including cost reduction, rapid prototyping, and efficient resource utilization.

The primary contributions of this study include filling the identified research gap regarding the application of 3D printing in sheet metal tooling and advancing the understanding of SLA/DLP technologies for tool optimization. Using Al99.5 and AlMg3 sheet materials under rigorous testing conditions, the research showed that printed tools can withstand repetitive mechanical stresses while maintaining structural integrity. The high precision and minimal wear observed indicate that DLP printing is a transformative tool-making technology.

Despite the promising outcomes, this study has several limitations. The experiments focused on a limited range of materials and production scales. Expanding the scope to include diverse alloys and higher production volumes is necessary to evaluate the broader industrial applicability of DLP tools. Furthermore, the wear resistance of the DLP-printed tools under extended operational cycles warrants deeper investigation.

Future research should aim to achieve the following goals:

1. Explore the use of advanced material compositions for DLP printing to enhance wear resistance and durability.
2. Investigate the impact of infill patterns on mechanical properties and optimize them for specific applications.
3. Integrate artificial intelligence techniques to predict tool wear, optimize print parameters, and streamline production processes [44–46].
4. Collaborate with industry partners to conduct field trials, ensuring the transferability of laboratory findings to real-world scenarios [6,16,40,42,47].

These advancements could significantly enhance the credibility and adoption of DLP technology in industrial settings, offering a sustainable, cost-effective alternative to traditional manufacturing methods.

Author Contributions: Conceptualization, S.S., B.F.S., V.N., G.S., D.K., M.S. and S.F.; methodology, S.S., B.F.S., V.N., G.S., D.K., M.S. and S.F.; software, S.S., B.F.S., V.N., G.S., D.K., M.S. and S.F.; validation, S.S., B.F.S., V.N., G.S., D.K., M.S. and S.F.; formal analysis, S.S., B.F.S., V.N., G.S., D.K., M.S. and S.F.; investigation, S.S., B.F.S., V.N., G.S., D.K., M.S. and S.F.; resources, S.S., B.F.S., V.N., G.S., D.K., M.S. and S.F.; data curation, S.S., B.F.S., V.N., G.S., D.K., M.S. and S.F.; writing—original draft preparation, S.S., B.F.S., V.N., G.S., D.K., M.S. and S.F.; writing—review and editing, S.S., B.F.S., V.N., G.S., D.K., M.S. and S.F.; visualization, S.S., B.F.S., V.N., G.S., D.K., M.S. and S.F.; supervision, S.S., B.F.S., V.N., G.S., D.K., M.S. and S.F.; project administration, S.S., B.F.S., V.N., G.S., D.K., M.S. and S.F.; funding acquisition, S.S., B.F.S., V.N., G.S., D.K., M.S. and S.F. All authors have read and agreed to the published version of the manuscript.

Funding: The publication of this paper did not receive financial support or financing of the article processing charge.

Data Availability Statement: The data are available within the paper.

Acknowledgments: The authors are related to the research team “SZE-RAIL”.

Conflicts of Interest: The authors declare no conflicts of interest.

Abbreviations

3D	three-dimensional;
AM	additive manufacturing;
CAD	computer-aided design;
cDLP	continuous digital light processing;
DIC	digital image correlation;
DLP	digital light processing;
FDM®	fused deposition modeling;
IT	international tolerance;
ISO	International Organization for Standardization;
MSLA	masked stereolithography apparatus;
PPP	pulse projection polymerization;
SLA	stereolithography apparatus;
STL	file format for stereolithography;
UV	ultraviolet.

Nomenclature

$A_{11.3}$	percentage strain at breakage (related to a $L_o = 10 \cdot d_0$ measuring basis);
d_0	original diameter or thickness of the sample/specimen before deformation;
H	cutting die height [mm];
s	thickness of the sheet (plate) [mm].

References

1. Klimyuk, D.; Serezhkin, M.; Plokhikh, A. Application of 3D Printing in Sheet Metal Forming. *Mater. Today Proc.* **2021**, *38*, 1579–1583. [CrossRef]
2. Dižo, J.; Blatnický, M.; Sága, M.; Harušinec, J.; Gerlici, J.; Legutko, S. Development of a New System for Attaching the Wheels of the Front Axle in the Cross-Country Vehicle. *Symmetry* **2020**, *12*, 1156. [CrossRef]
3. Volkov, V.; Taran, I.; Volkova, T.; Pavlenko, O.; Berezhnaja, N. Determining the Efficient Management System for a Specialized Transport Enterprise. *Nauk. Visnyk Natsionalnoho Hirnychoho Universytetu* **2020**, *2020*, 185–191. [CrossRef]
4. Saukenova, I.; Oliskevych, M.; Taran, I.; Toktamyssova, A.; Aliakbarkyzy, D.; Pelo, R. Optimization of Schedules for Early Garbage Collection and Disposal in the Megapolis. *East.-Eur. J. Enterp. Technol.* **2022**, *1*, 13–23. [CrossRef]
5. Tondini, F.; Basso, A.; Arinbjarnar, U.; Nielsen, C.V. The Performance of 3D Printed Polymer Tools in Sheet Metal Forming. *Metals* **2021**, *11*, 1256. [CrossRef]
6. Fischer, S.; Harangozó, D.; Németh, D.; Kocsis, B.; Sysyn, M.; Kurhan, D.; Brautigam, A. Investigation of Heat-Affected Zones of Thermite Rail Welding. *Facta Univ. Ser. Mech. Eng.* **2024**, *22*, 689–710. [CrossRef]
7. Banea, M.D.; da Silva, L.F. Adhesively bonded joints in composite materials: An overview. *Proc. Inst. Mech. Eng. Part L J. Mater. Des. Appl.* **2009**, *223*, 1–18. [CrossRef]
8. Kuchak, A.T.J.; Marinkovic, D.; Zehn, M. Parametric Investigation of a Rail Damper Design Based on a Lab-Scaled Model. *J. Vib. Eng. Technol.* **2021**, *9*, 51–60. [CrossRef]
9. Kuchak, A.T.J.; Marinkovic, D.; Zehn, M. Finite Element Model Updating—Case Study of a Rail Damper. *Struct. Eng. Mech.* **2020**, *73*, 27–35. [CrossRef]
10. Deng, W.; Xie, D.; Liu, F.; Zhao, J.; Shen, L.; Tian, Z. DLP-Based 3D Printing for Automated Precision Manufacturing. *Mob. Inf. Syst.* **2022**, *2022*, 2272699. [CrossRef]
11. Zaragoza, V.G.; Rane, K.; Strano, M.; Monno, M. Manufacturing and Performance of 3D Printed Plastic Tools for Air Bending Applications. *J. Manuf. Process.* **2021**, *66*, 460–469. [CrossRef]
12. Shanmugasundaram, S.A.; Razmi, J.; Mian, M.J.; Ladani, L. Mechanical Anisotropy and Surface Roughness in Additively Manufactured Parts Fabricated by Stereolithography (SLA) Using Statistical Analysis. *Materials* **2020**, *13*, 2496. [CrossRef]
13. Nakamura, N.; Mori, K.-I.; Abe, Y. Applicability of Plastic Tools Additively Manufactured by Fused Deposition Modelling for Sheet Metal Forming. *Int. J. Adv. Manuf. Technol.* **2020**, *108*, 975–985. [CrossRef]
14. Zaragoza, V.G.; Strano, M.; Iorio, L.; Monno, M. Sheet Metal Bending with Flexible Tools. *Procedia Manuf.* **2019**, *29*, 232–239. [CrossRef]
15. Szabó, B.; Pásthy, L.; Orosz, Á.; Tamás, K. The Investigation of Additive Manufacturing and Moldable Materials to Produce Railway Ballast Grain Analogs. *Frat. Integrità Strutt.* **2022**, *60*, 213–228. [CrossRef]
16. Ézsiás, L.; Tompa, R.; Fischer, S. Investigation of the Possible Correlations between Specific Characteristics of Crushed Stone Aggregates. *Spectr. Mech. Eng. Oper. Res.* **2024**, *1*, 10–26. [CrossRef]
17. Orzeł, B.; Stecuła, K. Comparison of 3D Printout Quality from FDM and MSLA Technology in Unit Production. *Symmetry* **2022**, *14*, 910. [CrossRef]
18. Naeem, O.A.; Bencharit, S.; Yang, I.H.; Stilianoudakis, S.C.; Carrico, C.; Tüfekçi, E. Comparison of 3-Dimensional Printing Technologies on the Precision, Trueness, and Accuracy of Printed Retainers. *Am. J. Orthod. Dentofac. Orthop.* **2022**, *161*, 582–591. [CrossRef]
19. Gaikwad, S.R.; Pawar, N.H.; Sapkal, S.U. Comparative Evaluation of 3D Printed Components for Deviations in Dimensional and Geometrical Features. *Mater. Today Proc.* **2022**, *59*, 297–304. [CrossRef]
20. Komissarenko, D.A.; Sokolov, P.S.; Evstigneeva, A.D.; Slyusar, I.V.; Nartov, A.S.; Volkov, P.A.; Lyskov, N.V.; Evdokimov, P.V.; Putlayev, V.I.; Dosovitsky, A.E. DLP 3D Printing of Scandia-Stabilized Zirconia Ceramics. *J. Eur. Ceram. Soc.* **2021**, *41*, 684–690. [CrossRef]
21. Park, S.M.; Park, J.M.; Kim, S.K.; Heo, S.J.; Koak, J.Y. Flexural Strength of 3D-Printing Resin Materials for Provisional Fixed Dental Prostheses. *Materials* **2020**, *13*, 3970. [CrossRef]
22. Truxova, V.; Safka, J.; Seidl, M.; Kovalenko, I.; Volesky, L.; Ackermann, M. Ceramic 3D Printing: Comparison of SLA and DLP Technologies. *MM Sci. J.* **2020**, *2020*, 3905–3911. [CrossRef]

23. Cosmi, F.; Dal Maso, A. A mechanical characterization of SLA 3D-printed specimens for low-budget applications. *Mater. Today Proc.* **2020**, *32*, 194–201. [CrossRef]
24. Nagaraju, D.S.; Krupakaran, R.; Sripadh, C.; Nitin, G.; Joy Joseph Emmanuel, G. Mechanical Properties of 3D Printed Specimen Using FDM (Fused Deposition Modelling) and SLA (Stereolithography) Technologies. *Mater. Today Proc.* 2023; *in press*. [CrossRef]
25. Li, Y.; Teng, Z. Effect of Printing Orientation on Mechanical Properties of SLA 3D-Printed Photopolymer. *Fatigue Fract. Eng. Mater. Struct.* **2024**, *47*, 1531–1545. [CrossRef]
26. Park, J.-M.; Jeon, J.; Koak, J.-Y.; Kim, S.-K.; Heo, S.-J. Dimensional Accuracy and Surface Characteristics of 3D-Printed Dental Casts. *J. Prosthet. Dent.* **2021**, *126*, 427–437. [CrossRef]
27. Tuteski, O.; Kočov, A. Tensile Strength and Dimensional Variances in Parts Manufactured by SLA 3D Printing. *Industry 4.0* **2021**, *6*, 143–149.
28. Stögerer, J.; Baumgartner, S.; Rath, T.; Stampfl, J. Analysis of the Mechanical Anisotropy of Stereolithographic 3D Printed Polymer Composites. *Eur. J. Mater.* **2022**, *2*, 12–32. [CrossRef]
29. Afteni, C.; Costin, G.; Iabob, I.; Păunoiu, V.; Teodor, V. A review on sheet metal rubber-pad forming. *Ann. "Dunarea De Jos" Univ. Galati Fascicle V Technol. Mach. Build.* **2018**, *36*, 49–54. [CrossRef]
30. Attila, B.; Gaszton, G. A Gumiszerszámos Lemezmegmunkálás. In *Fiatal Műszakiak Tudományos Üllésszaka*; Erdélyi Múzeum Egyesület (EME): Cluj, Romania, 1997.
31. Skriba, Z. *A Fémek Képlékeny Alakításának Technológiája*; Műszaki Könyvkiadó: Budapest, Hungary, 1976.
32. Végvári, F. Négyzetes Lyukasztás és Kivágás Poliuretán Párnával. In *Fiatal Műszakiak Tudományos Üllésszaka*; Erdélyi Múzeum Egyesület (EME): Kolozsvár, Romania, 2004.
33. *ASTM D792*; Standard Test Methods for Density and Specific Gravity (Relative Density) of Plastics by Displacement. ASTM International: West Conshohocken, PA, USA, 2020.
34. *ISO 1628-1:2021*; Plastics—Determination of the Viscosity of Polymers in Dilute Solution Using Capillary Viscometers. ISO: Geneva, Switzerland, 2021.
35. *ISO/TC 164/SC 3*; Hardness Testing. ISO: Geneva, Switzerland, 1981.
36. *ISO 527-1:2019*; Plastics—Determination of Tensile Properties. ISO: Geneva, Switzerland, 2019.
37. *ISO 180:2019*; Plastics—Determination of Izod Impact Strength. ISO: Geneva, Switzerland, 2019.
38. *ASTM D790*; Standard Test Methods for Flexural Properties of Unreinforced and Reinforced Plastics and Electrical Insulating Materials. ASTM International: Geneva, Switzerland, 2020.
39. Kampczyk, A.; Dybeł, K. Integrating Surveying Railway Special Grid Pins with Terrestrial Laser Scanning Targets for Monitoring Rail Transport Infrastructure. *Measurement* **2021**, *170*, 108729. [CrossRef]
40. Szívós, B.F.; Szalai, S.; Fischer, S. Deformation Test of 3D Printed Battery Case Using DIC Technology. In Proceedings of the International Conference on Electrical, Computer, Communications and Mechatronics Engineering (ICECCME 2023), Tenerife, Canary Islands, Spain, 19–21 July 2023; p. 10253004. [CrossRef]
41. Zaldivar, R.J.; Witkin, D.B.; McLouth, T.; Patel, D.N.; Schmitt, K.; Nokes, J.P. Influence of processing and orientation print effects on the mechanical and thermal behavior of 3D-Printed ULTEM® 9085 Material. *Addit. Manuf.* **2017**, *13*, 71–80. [CrossRef]
42. Szalai, S.; Herold, B.; Kurhan, D.; Németh, A.; Sysyn, M.; Fischer, S. Optimization of 3D Printed Rapid Prototype Deep Drawing Tools for Automotive and Railway Sheet Material Testing. *Infrastructures* **2023**, *8*, 43. [CrossRef]
43. *ISO 286-1:2010*; Geometrical Product Specifications (GPS)—ISO Code System for Tolerances on Linear Sizes. ISO: Geneva, Switzerland, 2010.
44. Ficzere, P. The Role of Artificial Intelligence in the Development of Rail Transport. *Cogn. Sustain.* **2023**, *2*, 81. [CrossRef]
45. Zamfirache, I.A.; Precup, R.E.; Petriu, E.M. Q-Learning, Policy Iteration and Actor-Critic Reinforcement Learning Combined with Metaheuristic Algorithms in Servo System Control. *Facta Univ. Ser. Mech. Eng.* **2023**, *21*, 615–630. [CrossRef]
46. Nosonovsky, M.; Aglikov, A.S. Triboinformatics: Machine Learning Methods for Frictional Instabilities. *Facta Univ. Ser. Mech. Eng.* **2024**, *22*, 423–433. [CrossRef]
47. Fischer, S. Investigation of the Settlement Behavior of Ballasted Railway Tracks Due to Dynamic Loading. *Spectr. Mech. Eng. Oper. Res.* **2025**, *2*, 24–46. [CrossRef]